Closed-Loop Control of a Three-Phase Neutral-Point-Clamped Inverter Using an Optimized Virtual-Vector-Based Pulsewidth Modulation

Sergio Busquets-Monge, *Member, IEEE*, José Daniel Ortega, Josep Bordonau, *Member, IEEE*, José Antonio Beristáin, and Joan Rocabert

***Abstract*—This paper presents a closed-loop control scheme for the three-level three-phase neutral-point-clamped dc–ac converter using the optimized nearest three virtual-space-vector pulsewidth modulation, which is a modulation that produces low output-voltage distortion with a significant reduction of the dc-link capacitance. A new specific loop modifying the modulating waveforms is proposed to rapidly control possible perturbations in the neutral-point voltage balance. An online estimation of the load displacement angle and load linear/nonlinear nature is introduced at no extra cost. The remaining part of the control is analogous to the control for a two-level converter with an appropriate interfacing to the selected modulation. The closed-loop control is designed for the case of a renewable-energy source connected to the ac mains, and its performance is analyzed through simulation and experiments.**

***Index Terms*—Multilevel, neutral-point voltage balancing, pulsewidth modulation (PWM), renewable-energy systems, space-vector modulation, three-level three-phase neutral-point-clamped (NPC) dc–ac converter, virtual vectors, wind-energy systems.**

I. Introduction

MULTILEVEL converters [1], [2] are currently a particularly active area of research [3]–[26] due to their significant advantages in electrical power conversion. In these topologies and compared with a two-level converter, the voltage across each semiconductor, the output-voltage harmonic distortion, and the converter losses are reduced. However, a larger number of semiconductors are needed, and the modulation strategy to control them becomes more complex.

Multilevel converters are typically considered for high-power applications because they allow operations at higher dc-link voltage levels, avoiding the problems of the series interconnection of devices. It has been recently reported that they present better efficiency than other alternative topologies [20]. Moreover, they can also be interesting for medium- or even low-power/voltage applications because they allow operations with lower voltage-rated devices, which is with potentially better performance/economical features [27], [28].

Among these topologies, the three-level three-phase neutral-point-clamped (NPC) dc–ac converter [29], which is shown in Fig. 1(a), is probably the most popular. The application of conventional modulation techniques to this converter causes a low-frequency (around three times the fundamental frequency of the output voltage, $f_o = 1/T_o$) oscillation of the neutral-point voltage. This, in turn, increases the voltage stress on the devices and generates low-order harmonics in the output voltage.

There have been many efforts to analyze this problem and define a modulation strategy to solve it [4], [26], [30]–[40], thereby eliminating the need to significantly increase the dc-side capacitance to minimize the voltage oscillation.

Among them, the nearest three virtual-space-vector (NTV^2) pulsewidth modulation (PWM) [39] allows the control of the neutral-point voltage over the full range of converter-output voltages and for any load. The optimized NTV^2 (ONTV^2) PWM [40] also allows one to comprehensively control the neutral-point voltage but with a lower output-voltage harmonic distortion in the case of linear-and-balanced ac loads.

The design of a closed-loop control scheme interfacing the ONTV^2 PWM is not straightforward: on the one hand, because the modulation scheme is defined in $d-q-0$ coordinates and, on the other hand, because there is a need to introduce a closed loop modifying the modulating waveforms in order to correct possible dc-link capacitor-voltage-balance perturbations. Additionally, an online estimation of the load displacement angle and linear/nonlinear nature is needed. This paper presents a proposal of such control for a renewable-energy system, which is without the loss of generality, and the performance of the proposed control scheme is verified through simulation and experiments.

This paper is organized as follows. Section II presents a summary of the core modulation strategy. Section III describes the closed-loop control, which is designed for the specific case of the connection of a renewable-energy source to the grid. Section IV presents simulation and experimental results to verify the good system performance. Finally, Section V outlines the conclusions.

Manuscript received September 7, 2007; revised January 9, 2008. This paper was presented in part at IEEE PESC'06. This work was supported by the Ministerio de Educación y Ciencia, Spain, under Grant TEC2005-08042.

S. Busquets-Monge, J. Bordonau, and J. Rocabert are with the Department of Electronic Engineering, Technical University of Catalonia, 08028 Barcelona, Spain (e-mail: sergio.busquets@upc.edu).

J. D. Ortega was with the Department of Electronic Engineering, Technical University of Catalonia, 08028 Barcelona, Spain. He is now with Adisa Calefacción S. L., 08006 Barcelona, Spain (e-mail: jdocastillo@hotmail.com).

J. A. Beristáin is with the Electrical and Electronic Engineering Department, Technological Institute of Sonora, 85000 Sonora, Mexico (e-mail: bantonio@itson.mx).

Color versions of one or more of the figures in this paper are available online at http://ieeexplore.ieee.org.

Digital Object Identifier 10.1109/TIE.2008.918646

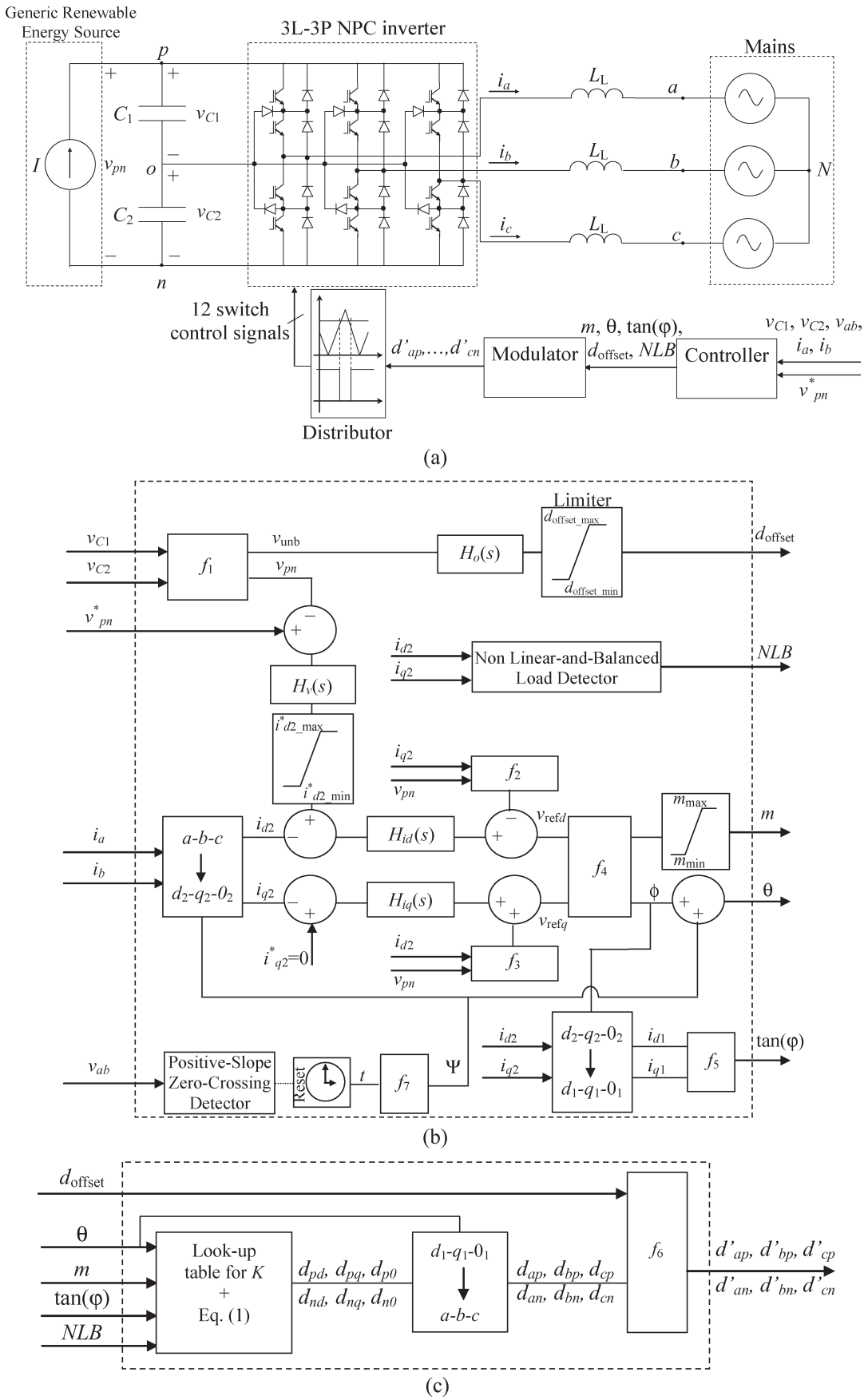

Fig. 1. System block diagram. (a) Power stage plus control. (b) Controller structure. (c) Modulator structure.

II. ONTV^2 PWM

Let us designate d_{ap}, d_{bp}, d_{cp}, d_{an}, d_{bn}, and d_{cn} as the six independent converter phase duty ratios, where d_{xy} refers to the duty ratio of the phase x connection to the dc-link point y. Equation (1), which is shown at the bottom of the page, reproduces from [40] the six expressions that define the ONTV^2 PWM in terms of these six independent converter phase duty ratios in the $d{-}q{-}0$ coordinates (d_{pd}, d_{pq}, d_{p0}, d_{nd}, d_{nq}, and d_{n0}), where $m(\in [0,1])$ and θ are, respectively, the length and angle (with reference to the axis α, which is aligned with the vector $\mathbf{V}_{\mathrm{L1}}$ corresponding to switching state pnn [39]) of the reference vector $\mathbf{V}_{\mathrm{ref}}$, which is a rotating vector in the converter space-vector plane that represents the desired fundamental converter-output three-phase voltage. The expressions in (1) assume that the axis d of the $d{-}q{-}0$ transformation of the phase duty ratios is aligned with $\mathbf{V}_{\mathrm{ref}}$. The variable φ is the ac load/source displacement angle, and the optimum value of the parameter K is a function of m and φ. In [40], expressions are provided to compute the value of K as a function of m and φ. Alternatively, a lookup table as a function of m and $\tan(\varphi)$ can be generated to select the appropriate value of K online.

Given the values of m, θ, and $\tan(\varphi)$, the duty ratios in the $d{-}q{-}0$ coordinates can be obtained from (1) and the look-up table or expressions to compute K. Applying the inverse $d{-}q{-}0$ transformation, we then obtain the independent phase duty ratios d_{ap}, d_{bp}, d_{cp}, d_{an}, d_{bn}, and d_{cn}. From these duty ratios and assuming that the sequence within a switching cycle of connection of each phase to each of the dc-link points is the symmetrical $p{-}o{-}n{-}o{-}p$, it is fairly straightforward to generate the 12 switch control signals.

III. Closed-Loop Control Design

The proposed modulator and controller have been designed and implemented for the particular system in Fig. 1(a). The purpose of the system is to send the energy from a renewable-energy source to the mains with a unity displacement factor while also regulating the voltage ν_{pn}. The closed-loop control designed is applicable to any system where the power source can be basically modeled as a current source and the energy is sent to the mains, such as a wind-energy conversion system where the ac generator is connected to a noncontrolled boost rectifier [41]. The diagrams of Fig. 1(b) and (c) show the proposed controller and modulator structure, which is discussed in detail in the following sections.

A. Neutral-Point Voltage Control

The ONTV^2 PWM guarantees no low-frequency oscillations of $\nu_{\mathrm{unb}} = (\nu_{C_2} - \nu_{C_1})/2$ due to the loading conditions of the converter, provided that the addition of line currents equals zero. Even if the load presents a severe nonlinearity or unbalance, this will not affect the dc-link voltage balance if we set $K = 0$. The occurrence of neutral-point voltage perturbations should, however, be considered. Perturbations can occur if, for example, there is a leakage current flowing from the load neutral to ground, causing the addition of the three-phase currents to be different from zero. The nonidealities and, particularly, the differences in the switching behavior of the converter devices are another possible source of disturbances.

As discussed in [42], certain modulations have the property of naturally recovering the dc-link voltage balance after a perturbation in the absence of a dedicated control action. The ONTV^2 PWM with $K = 0$ does not belong to this family of modulations. It does not affect the balance of the dc-link capacitor voltages. If an unbalance exists at a given point in time, the ONTV^2 PWM with $K = 0$ will preserve this unbalance [see Fig. 2(a)]. However, the ONTV^2 with $K > 0$ belongs to the set of modulations that naturally recover the balance [see Fig. 2(b)]. The higher the value of K, the faster the system recovers the balance. Nevertheless, this natural recovery process is usually slow.

The addition of discharging resistors to the dc-link capacitors also helps recovering the balance after a perturbation. Their resistance value is usually high, however, and the recovery process, thanks to these resistors, is also slow.

Considering that all preexisting possible balance recovery processes do not seem to be effective/fast enough, an

$$
\begin{aligned}
d_{pq} &= -K \cdot \sin(3 \cdot \theta) \\
d_{pd} &= \tan(\varphi) \cdot d_{pq} + m/\sqrt{2} \\
d_{nd} &= d_{pd} - \sqrt{2} \cdot m \\
d_{nq} &= d_{pq} \\
&\begin{cases}
\theta \le 2\pi/3: & d_{p0} = \sqrt{2} \cdot (-d_{pd} \cdot \cos(\theta + 2\pi/3) + d_{pq} \cdot \sin(\theta + 2\pi/3)) \\
2\pi/3 < \theta \le 4\pi/3: & d_{p0} = \sqrt{2} \cdot (-d_{pd} \cdot \cos(\theta) + d_{pq} \cdot \sin(\theta)) \\
\theta > 4\pi/3: & d_{p0} = \sqrt{2} \cdot (-d_{pd} \cdot \cos(\theta - 2\pi/3) + d_{pq} \cdot \sin(\theta - 2\pi/3))
\end{cases} \\
&\begin{cases}
\theta \le \pi/3, \theta > 5\pi/3: & d_{n0} = \sqrt{2} \cdot (-d_{nd} \cdot \cos(\theta) + d_{nq} \cdot \sin(\theta)) \\
\pi/3 < \theta \le \pi: & d_{n0} = \sqrt{2} \cdot (-d_{nd} \cdot \cos(\theta - 2\pi/3) + d_{nq} \cdot \sin(\theta - 2\pi/3)) \\
\pi < \theta \le 5\pi/3: & d_{n0} = \sqrt{2} \cdot (-d_{nd} \cdot \cos(\theta + 2\pi/3) + d_{nq} \cdot \sin(\theta + 2\pi/3))
\end{cases}
\end{aligned}
\tag{1}
$$

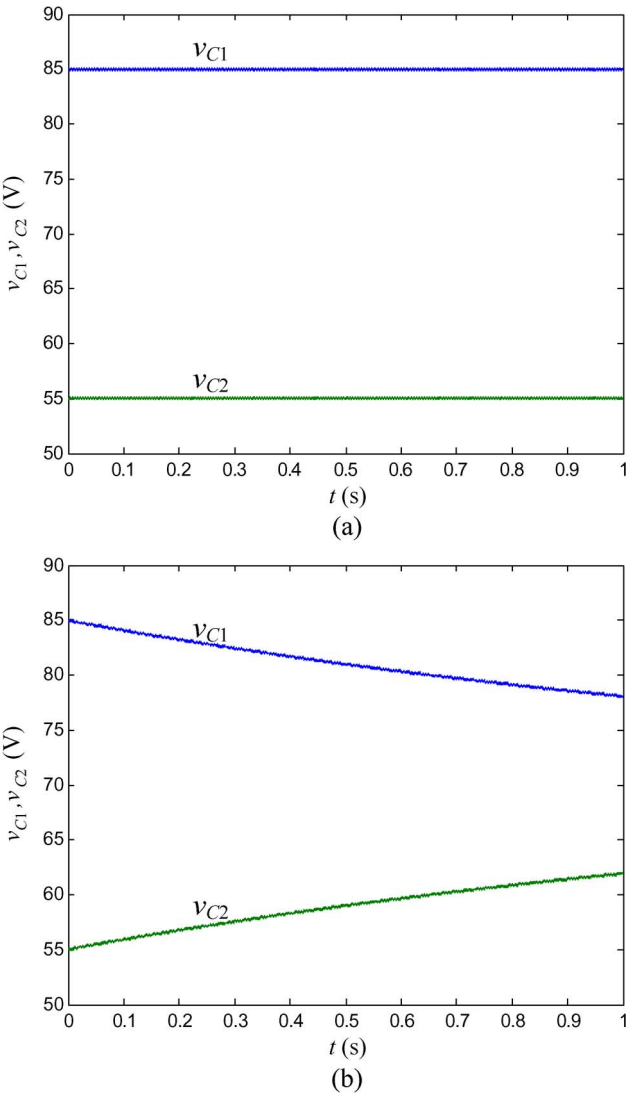

Fig. 2. Natural dc-link capacitor voltage balance recovery transient in the following conditions: $V_{pn} = 140$ V, $m = 0.75$, $f_o = 50$ Hz, switching frequency $f_s = 5$ kHz, $C_1 = C_2 = 1.1$ mF, and a wye-connected three-phase RL load ($R_L = 16.5\ \Omega, L_L = 5$ mH). (a) ONTV^2 PWM, $K = 0$. (b) ONTV^2 PWM, $K = 0.1$.

appropriate perturbation of the modulating waveforms that allowed one to speed up this process would be helpful.

In the most recent literature, a few proposals for the balancing of three-level three-phase diode-clamped converters have been presented [19], [22], [23]. Reference [22] studies the case of a dual multilevel converter, and hence, the topology differs from the single multilevel converter considered here [Fig. 1(a)]. Reference [23] applies a predictive strategy to control the NPC converter and, in particular, to guarantee the dc-link capacitor voltage balance. However, this strategy requires *a priori* knowledge of the converter load model and leads to a spread spectrum in the output voltage, making the filtering of the output-voltage distortion a challenge. Reference [19] studies the control of the NPC converter with a modulation scheme in essence, which is equivalent to the NTV^2 PWM presented in [39] (ONTV^2 PWM with $K = 0$). To correct any dc-link capacitor voltage unbalance at any given switching cycle, the phase duty ratios of only one phase are perturbed. The phase x being perturbed is the one verifying $d_{xp} > 0$ and $d_{xn} > 0$. The duty ratios d_{xp} and d_{xn} are both increased (or decreased, depending on the sign of the voltage unbalance and the phase current) the same quantity, in order to recover the balance.

A different control solution is proposed in this paper, which is applicable to the general ONTV^2 PWM. It presents several advantages over the solution in [19], which are discussed at the end of this section. Reference [33] shows that introducing a common-mode voltage into all three line-to-neutral output-voltage waveforms causes an unbalance in the discharging of the dc-link capacitors. This property can be used to speed up the recovery process whenever a dc-link voltage unbalance occurs. In this paper, this control mechanism is adapted to the ONTV^2 PWM.

A priori, it is not clear which modulating waveforms need to be modified to introduce this common-mode voltage, considering that there are two (instead of one) modulating waveforms per phase (d_{xp} and d_{xn}). An offset (d_{offset}) has to be added to all three $d_{ap}-d_{an}$, $d_{bp}-d_{bn}$, and $d_{cp}-d_{cn}$ modulating waveforms. There are three options in adding an offset to the $d_{xp}-d_{xn} (x \in \{a, b, c\})$ waveform.

1) Add the offset to d_{xp}.
2) Subtract the offset from d_{xn}.
3) Add part of the offset to d_{xp}, and subtract the remaining part from d_{xn}.

A simple and interesting strategy is to apply all the offsets to the duty ratio to be reduced. Considering that the duty ratios must be greater than zero, in case this duty ratio reaches the value of zero, the other duty ratio will be increased a quantity corresponding to the part of the offset that is still not applied. This strategy allows the minimization of the number of commutations because it will maximize the occasions where a nonzero duty ratio becomes zero. With reference to Fig. 1(c), this strategy can be formulated for phase x as

$$
\begin{aligned}
&d'_{ap} = f_{61}(d_{ap}, d_{an}, d_{\text{offset}}) \quad d'_{an} = f_{62}(d_{ap}, d_{an}, d_{\text{offset}})\\
&d'_{bp} = f_{63}(d_{bp}, d_{bn}, d_{\text{offset}}) \quad d'_{bn} = f_{64}(d_{bp}, d_{bn}, d_{\text{offset}})\\
&d'_{cp} = f_{65}(d_{cp}, d_{cn}, d_{\text{offset}}) \quad d'_{cn} = f_{66}(d_{cp}, d_{cn}, d_{\text{offset}})\\
&\textbf{if}(d_{\text{offset}} \geq 0)\\
&\quad \{\textbf{if}\ (d_{xn} > d_{\text{offset}})\\
&\qquad \{d'_{xn} = d_{xn} - d_{\text{offset}}\\
&\qquad\ d'_{xp} = d_{xp}\}\\
&\quad \textbf{else}\\
&\qquad \{d'_{xn} = 0\\
&\qquad\ d'_{xp} = d_{xp} + (d_{\text{offset}} - d_{xn})\}\}\\
&\textbf{else}\\
&\quad \{\textbf{if}\ (d_{xp} > |d_{\text{offset}}|)\\
&\qquad \{d'_{xp} = d_{xp} - |d_{\text{offset}}|\\
&\qquad\ d'_{xn} = d_{xn}\}\\
&\qquad \textbf{else}\\
&\qquad\ \{d'_{xp} = 0\\
&\qquad\ d'_{xn} = d_{xn} + (|d_{\text{offset}}| - d_{xp})\}\}.
\end{aligned}
\tag{2}
$$

The value of d_{offset} to be applied is determined by a compensator from the dc-link capacitor voltage unbalance $\nu_{\text{unb}} = f_{11}(\nu_{C_1}, \nu_{C_2}) = (\nu_{C_2} - \nu_{C_1})/2$. This compensator must have a low-pass characteristic in order to react only to perturbations

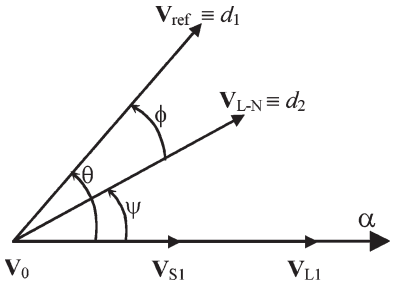

Fig. 3. Location of vectors $\mathbf{V}_{\text{ref}}$ and $\mathbf{V}_{\text{L}-\text{N}}$ that is with reference to the axis α.

Fig. 4. Three-level three-phase NPC dc–ac converter employed in the experiments. The converter is built with modules SKM 100 GB 123 D, SKM 100 GAL 123 D, and SKM 100 GAR 123 D (1200-V/100-A isolated-gate bipolar transistors). Voltage sensors: ABB VS 500 B. Current sensors: LEM LA 205 S.

in the dc-link voltage balance with frequencies lower than the switching frequency. The sign of d_{offset} must change if the direction of the power flow (ac to dc or dc to ac) changes. In applications where the direction of the power flow can vary, this variable must be monitored to guarantee a proper control action.

Compared with the control in [19], the control proposed here presents the following advantages.

1) It is applicable to the ONTV^2 PWM, which is for all values of K;
2) It has a stronger balancing action because, at any given switching cycle, all three phases are being perturbed to recover the balance instead of only one, and the balancing action is not limited to the minimum value (or one minus the maximum value) of the phase duty ratios involved.
3) It has lower number of switching transitions, considering that the offset is applied first through the phase duty ratios to be reduced. This will maximize the occasions where a nonzero duty ratio becomes zero, reducing the number of switching transitions.
4) It does not require the sensing of the phase currents in unidirectional power-flow applications.

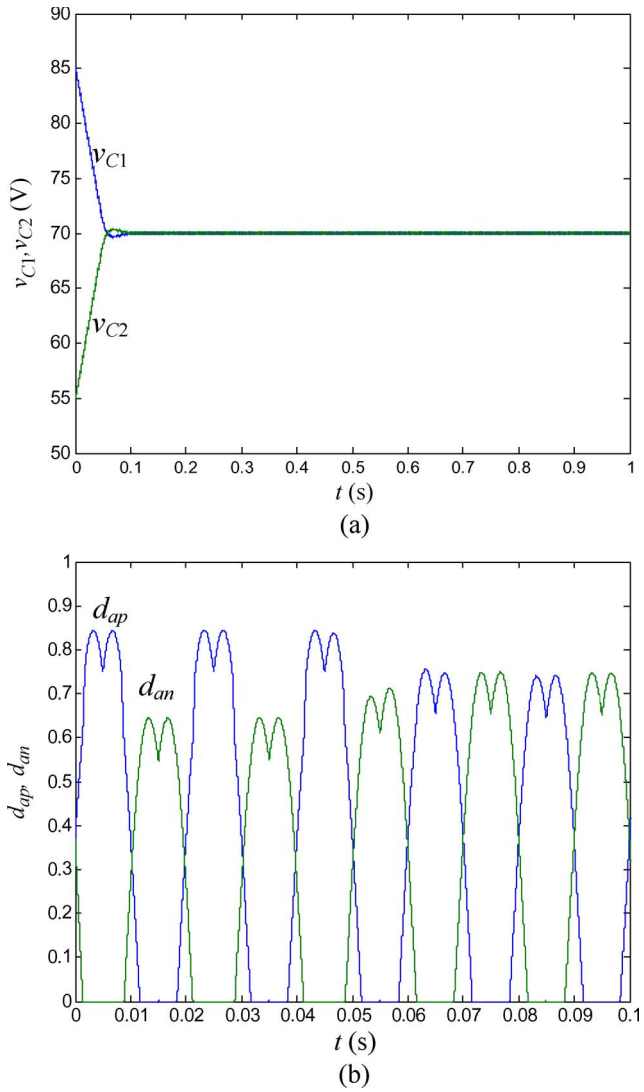

Fig. 5. DC-link capacitor voltage balance recovery transient in the conditions of Fig. 2(a) but with the dedicated neutral-point voltage control activated. (a) DC-link voltages ν_{C_1} and ν_{C_2}. (b) Phase-a independent duty ratios.

B. Non Linear-and-Balanced Load Detector

Whenever the load is not linear and balanced, we must set $K = 0$ in order to maintain the neutral-point voltage control. This situation can be detected by monitoring the maximum length of the line-current vector oscillation in the $d-q$ coordinates and, if it goes beyond a given maximum, activating and latching a non linear-and-balanced load flag (NLB) in order to force $K = 0$ in the modulator. The value of the Boolean variable NLB $(\in \{0, 1\})$ can be determined according to

$$\begin{aligned}
&\text{NLB} = 0, \qquad \text{if } \sqrt{\hat{i}_{d_2}^2 + \hat{i}_{q_2}^2} \le \hat{i}_{\max} \\
&\text{NLB} = 1, \qquad \text{if } \sqrt{\hat{i}_{d_2}^2 + \hat{i}_{q_2}^2} > \hat{i}_{\max} \\
&\hat{i}_{d_2}(t) = i_{d_2}(t) - \frac{1}{T_o} \int_{t-T_o}^{t} i_{d_2}(t) \cdot dt \\
&\hat{i}_{q_2}(t) = i_{q_2}(t) - \frac{1}{T_o} \int_{t-T_o}^{t} i_{q_2}(t) \cdot dt
\end{aligned} \tag{3}$$

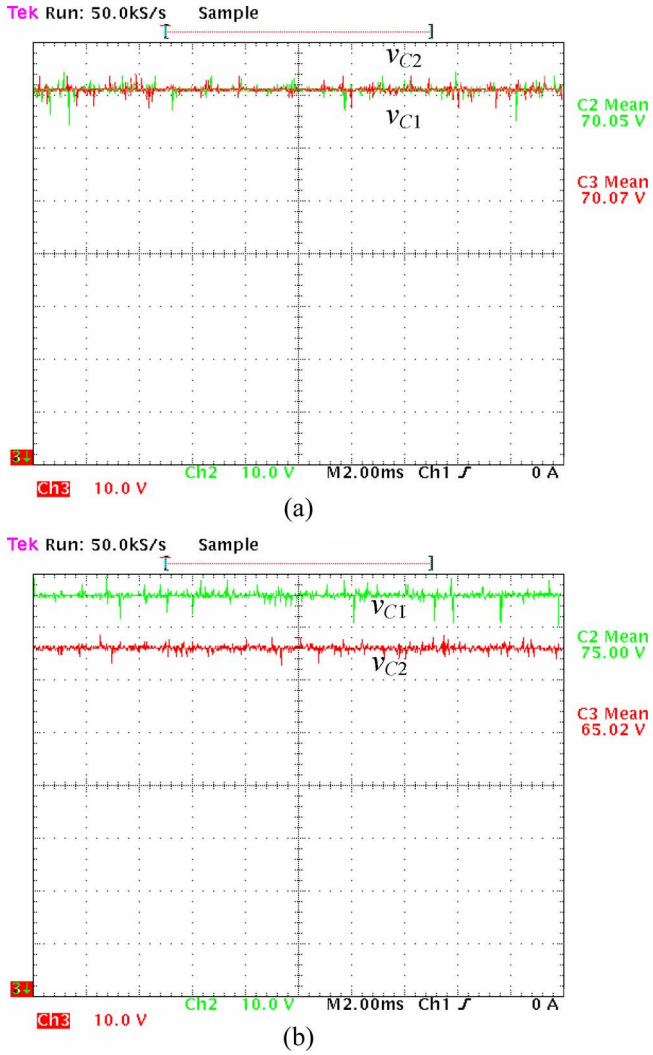

Fig. 6. Neutral-point voltage control performance in the conditions of Fig. 5. Control tuned to achieve (a) $\nu_{\rm unb} = 0$ V and (b) $\nu_{\rm unb} = -5$ V.

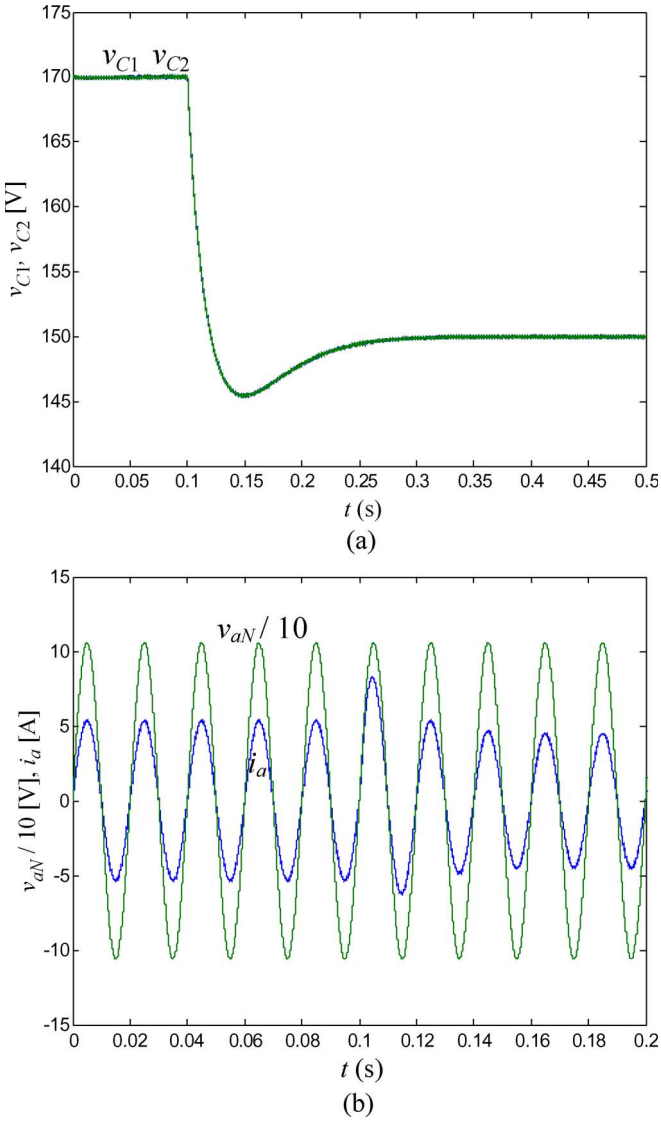

Fig. 7. Simulation results for a step in command ν^*_{pn} at time = 0.1 s in the following conditions: $I = 2.5$ A, $C_1 = C_2 = 1.1$ mF, $L_{\rm L} = 10$ mH, $V_{aN} = V_{bN} = V_{cN} = 75$ $V_{\rm rms}$, $f_o = 50$ Hz, and $f_{\rm s} = 5$ kHz. (a) DC-link voltages ν_{C_1} and ν_{C_2}. (b) Mains voltage ν_{aN} and line current i_a.

where $\hat{i}_{\max}$ is a constant representing the maximum length of the line-current vector oscillation in the $d-q$ coordinates.

C. Reference-Vector Computation

From a closed-loop control point of view, the key difference between a two- and a three-level dc–ac converter is that the latter introduces the dynamics of the neutral-point voltage. We can assume that the neutral-point voltage is always balanced, thanks to the chosen modulation and the dedicated control presented previously. Then, the average model of the three-level converter becomes equivalent to the model of a two-level converter. Hence, conventional control schemes and design procedures for the two-level converter can be directly applied to the three-level converter to obtain, from the sensed variables, the reference-vector length m and the angle θ required by the modulator.

For the particular application considered in this paper, the selected control scheme is shown in Fig. 1(b). First, the dc-link voltage $\nu_{pn} = f_{12}(\nu_{C_1}, \nu_{C_2}) = \nu_{C_1} + \nu_{C_2}$ is compared with the desired command. The error is then processed by a compensator to produce the i_d command. Line currents i_a and i_b are sensed, and $d-q$ is transformed. We do not need to sense i_c because we know $i_c = -i_a - i_b$. The transformation is performed to axes $d_2 - q_2 - 0_2$, where the axis d_2 is in phase with the vector of line-to-neutral mains voltages ($\mathbf{V}_{\rm L-N}$). This vector has an angle ψ with reference to the axis α (Fig. 3)

$$\psi = f_7(t) = \omega_o \cdot t - 2\pi/3 = 2\pi \cdot f_o \cdot t - 2\pi/3. \qquad (4)$$

The d_2 and q_2 components of the current are compared with their corresponding command. The i_{q_2} command is zero to achieve a unity displacement factor for the power transferred to the mains. Both the d and q channel errors are processed by their

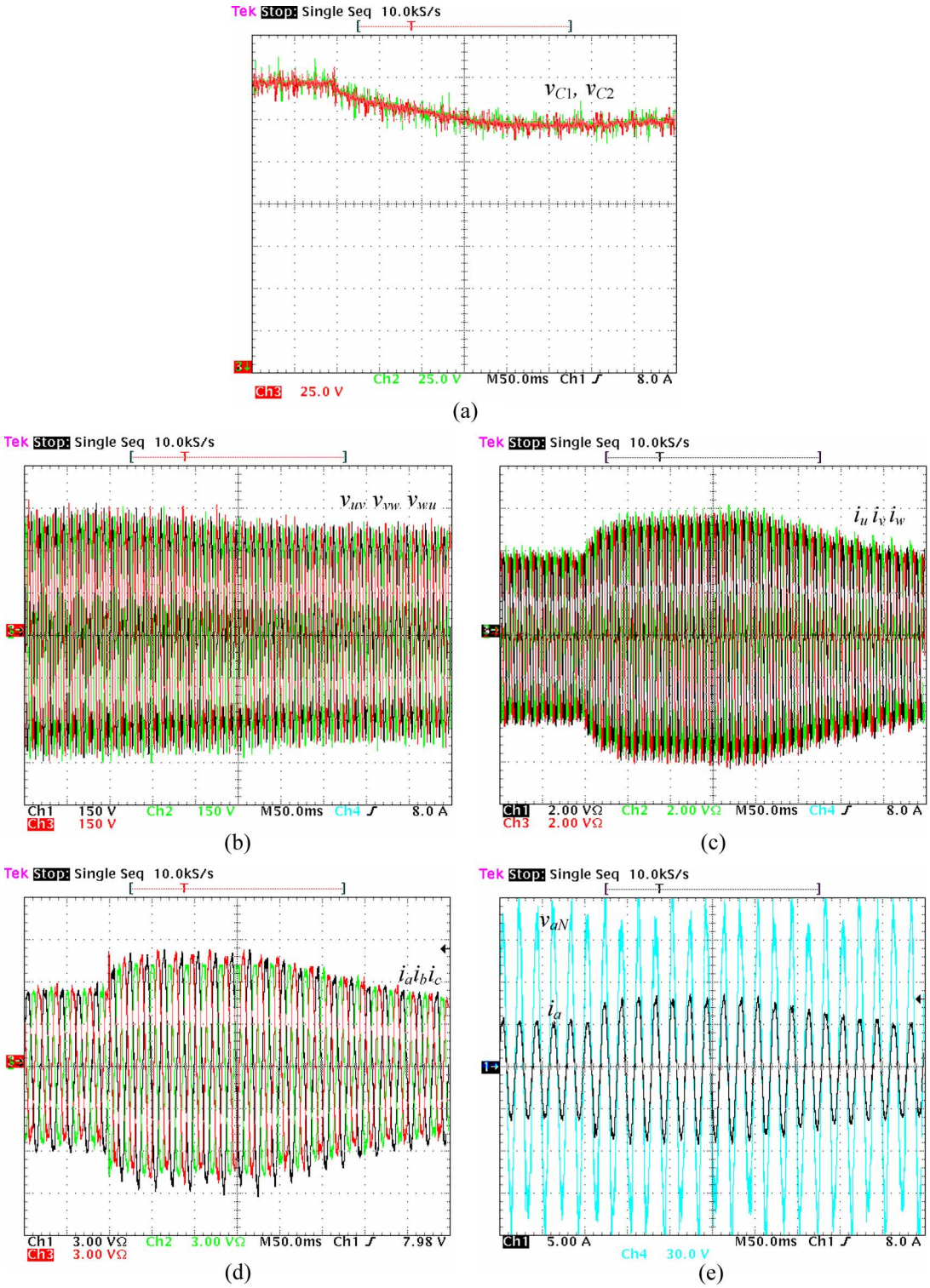

Fig. 8. Experimental results for a step in command ν_{pn}^{*} from 340 to 300 V (variation of rotor speed is from 1577 to 1396 r/min). Conditions are as follows: rectified windmill generator voltage, constant torque applied to the generator shaft = 10 Nm, $L_{\rm S} = 12.5$ mH, $C_1 = C_2 = 1.1$ mF, $L_{\rm L} = 10$ mH, $V_{aN} = V_{bN} = V_{cN} = 75$ $\rm V_{rms}$, $f_o = 50$ Hz, and $f_{\rm s} = 5$ kHz. (a) DC-link voltages ν_{C_1} and ν_{C_2} (25 V/div). (b) Generator line-to-line voltages $\nu_{u\nu}$, $\nu_{\nu w}$, and ν_{wu} (150 V/div). (c) Generator currents i_u, i_ν, and i_w (2 A/div). (d) i_a, i_b, and i_c (3 A/div). (e) Mains voltage ν_{aN} (30 V/div) and line current i_a (5 A/div).

specific compensators. Finally, both channels are decoupled through f_2 and f_3

$$f_2(i_{q_2}, \nu_{pn}) = \left(\sqrt{2} \cdot i_{q_2} \cdot \omega_o \cdot L_{\rm L}\right) / \nu_{pn}$$
$$f_3(i_{d_2}, \nu_{pn}) = \left(\sqrt{2} \cdot i_{d_2} \cdot \omega_o \cdot L_{\rm L}\right) / \nu_{pn}. \quad (5)$$

The outcome of both channels are the d_2 and q_2 components of $\mathbf{V}_{\rm ref}$. Through f_4, we obtain the $\mathbf{V}_{\rm ref}$ length m (modulation index) and angle ϕ (with reference to the axis d_2)

$$m = f_{41}(\nu_{{\rm ref}d}, \nu_{{\rm ref}q}) = \sqrt{\nu_{{\rm ref}d}^2 + \nu_{{\rm ref}q}^2}$$
$$\phi = f_{42}(\nu_{{\rm ref}d}, \nu_{{\rm ref}q}) = \tan^{-1}(\nu_{{\rm ref}q}/\nu_{{\rm ref}d}). \quad (6)$$

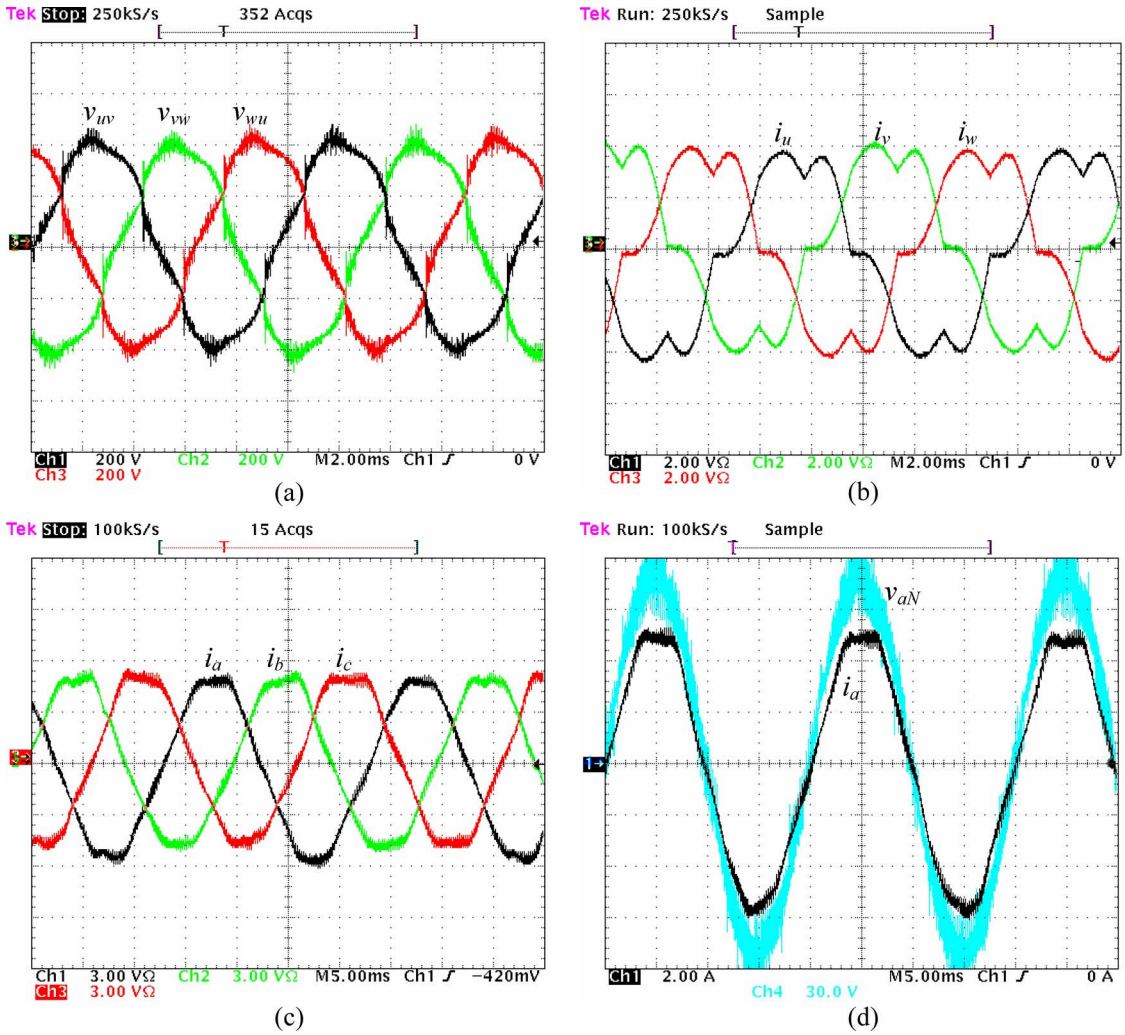

Fig. 9. Zoom-in views of Fig. 8(b)–(e) before the step in ν_{pn}^*. (a) Generator line-to-line voltages $\nu_{u\nu}$, $\nu_{\nu w}$, and ν_{wu} (200 V/div). (b) Generator currents i_u, i_ν, and i_w (2 A/div). (c) i_a, i_b, and i_c (3 A/div). (d) Mains voltage ν_{aN} (30 V/div) and line current i_a (2 A/div).

The angle θ can then be obtained by simply adding ψ and ϕ (Fig. 3). This is the angle that will be used to perform the transformation of the duty ratios from $d_1{-}q_1{-}0_1$ to $a{-}b{-}c$ coordinates within the modulator.

D. Online Estimation of the Load Displacement Angle

To implement the ONTV^2 PWM, we need an estimate of $\tan(\varphi)$. The angle φ corresponds to the angle between the vector of fundamental line currents and $\mathbf{V}_{\rm ref}$. Hence, the value of $\tan(\varphi)$ can be computed online by simply sensing the line currents, applying the $d_1{-}q_1$ transformation and using (7) (in the case of non linear-and-balanced loads, the dc values of the d_1 and q_1 components can be used). Considering that in general, the controller already requires sensing of the line currents, the implementation of the ONTV^2 PWM does not require additional sensors

$$\tan(\varphi) = f_5(i_{d_1}, i_{q_1}) = -i_{q_1}/i_{d_1}. \tag{7}$$

IV. Simulation and Experimental Results

Simulations have been carried out in Simulink with the closed-loop switching and average models of the system. For the experimental validation, the prototype in Fig. 4 has been employed. The controller and modulator blocks have been implemented with a PowerPC (dSPACE 1103) and the distributor block using a field-programmable gate array (Altera EPF10K70) [43]. In Figs. 5 and 6, the converter ac side is connected to a three-phase RL load. In Figs. 7–9, the converter is connected to the mains, as shown in Fig. 1(a).

Fig. 5(a) shows the advantage of introducing the neutral-point voltage control. The simulation has been performed in the same conditions as in Fig. 2(a). Fig 5(b) shows the modified duty-ratio pattern during the transient. Fig. 6 shows the good performance achieved with this control in the experiments. In Fig. 6(a), the control effort is negligible, where $d_{\rm offset} \cong -0.001$. In Fig. 6(b), $d_{\rm offset} \cong -0.01$.

The complete control has been tested through simulation in the conditions of Fig. 7. These results have been obtained with the complete closed-loop switching model for a step in

voltage command ν_{pn}^{*} from 340 to 300 V. We can observe that there is no unbalance of the dc-link capacitor voltages before, during, and after the step transient, which is as expected [Fig. 7(a)]. Considering that the ONTV^2 PWM already guarantees this balancing, the effort of the dedicated control is minimal $(-0.001 < d_{\mathrm{offset}} < 0.001)$. In Fig. 7(b), we can observe that the power conversion is achieved with a unity displacement factor, which is as intended.

Fig. 8 shows the experimental results obtained with an emulator of a wind-energy conversion system connected to the ac mains [Fig. 1(a)]. Fig. 9 shows zoom-in views of Fig. 8(b)–(e). The voltage of a windmill generator is connected to the inverter dc-link through a set of three line inductances (L_{S}) and a three-phase diode rectifier. A constant torque of 10 Nm is applied to the generator shaft to emulate the wind torque. A step in ν_{pn}^{*} from 340 to 300 V is forced, producing a variation of the rotor speed from 1577 to 1396 r/min. The controller employed is defined as

$$H_o(s) = -2 \cdot \frac{(s + 2\pi \cdot 0.01)}{s \cdot (s + 2\pi \cdot 25)}$$

$$H_\nu(s) = -1000 \cdot \frac{(s + 2\pi \cdot 5)}{s \cdot (s + 2\pi \cdot 2500)}$$

$$H_{id}(s) = 500 \cdot \frac{(s + 2\pi \cdot 25)}{s \cdot (s + 2\pi \cdot 2500)}$$

$$H_{iq}(s) = 1000 \cdot \frac{(s + 2\pi \cdot 5)}{s \cdot (s + 2\pi \cdot 2500)}$$

$$[d_{\mathrm{offset\_min}}, d_{\mathrm{offset\_max}}] = [-0.1, 0.1]$$

$$[i_{d_2\_\mathrm{min}}^{*}, i_{d_2\_\mathrm{max}}^{*}] = [-10, 10]$$

$$[m_{\mathrm{min}}, m_{\mathrm{max}}] = [0, 1]. \tag{8}$$

The mains voltages (ν_{aN}, ν_{bN}, and ν_{cN}) have been obtained by connecting an isolation transformer and an autotransformer to the public grid. The distortion and asymmetry of the obtained three voltages [see Figs. 8(e) and 9(d)] produce the distortion that can be appreciated in the output phase currents. Despite these nonidealities, the results show an overall good performance of the complete control, which guarantees the dc-link capacitor voltage balance and unity displacement factor during the entire transient.

V. Conclusion

A closed-loop control scheme for the three-level three-phase NPC dc–ac converter using the ONTV^2 PWM has been presented. The selected modulation allows one to use small dc-link capacitors, leading to an improved performance of the closed-loop system. A new specific control loop has been designed to speed up the recovery from neutral-point voltage perturbations. An online estimation of the load displacement angle and load linear/nonlinear nature is introduced at no extra cost. The remaining part of the control is analogous to the control for a two-level converter with an appropriate interfacing to the selected modulation. The good performance of the proposed control has been verified through simulation and experiments.

References

[1] J. Rodríguez, J. Lai, and F. Peng, "Multilevel inverters: A survey of topologies, controls and applications," *IEEE Trans. Ind. Electron.*, vol. 49, no. 4, pp. 724–738, Aug. 2002.

[2] L. Demas, T. A. Meynard, H. Foch, and G. Gateau, "Comparative study of multilevel topologies: NPC, multicell inverter and SMC with IGBT," in *Proc. IEEE Ind. Electron. Soc. Conf.*, 2002, vol. 1, pp. 828–833.

[3] L. G. Franquelo, M. A. M. Prats, R. C. Portillo, J. I. L. Galvan, M. A. Perales, J. M. Carrasco, E. G. Diez, and J. L. M. Jimenez, "Three-dimensional space-vector modulation algorithm for four-leg multilevel converters using abc coordinates," *IEEE Trans. Ind. Electron.*, vol. 53, no. 2, pp. 458–466, Apr. 2006.

[4] A. Bendre, G. Venkataramanan, D. Rosene, and V. Srinivasan, "Modeling and design of a neutral-point voltage regulator for a three-level diode-clamped inverter using multiple-carrier modulation," *IEEE Trans. Ind. Electron.*, vol. 53, no. 3, pp. 718–726, Jun. 2006.

[5] R. C. Portillo, M. M. Prats, J. I. Leon, J. A. Sanchez, J. M. Carrasco, E. Galvan, and L. G. Franquelo, "Modeling strategy for back-to-back three-level converters applied to high-power wind turbines," *IEEE Trans. Ind. Electron.*, vol. 53, no. 5, pp. 1483–1491, Oct. 2006.

[6] S. Alepuz, S. Busquets-Monge, J. Bordonau, J. Gago, D. Gonzalez, and J. Balcells, "Interfacing renewable energy sources to the utility grid using a three-level inverter," *IEEE Trans. Ind. Electron.*, vol. 53, no. 5, pp. 1504–1511, Oct. 2006.

[7] Y. Cheng, C. Qian, M. L. Crow, S. Pekarek, and S. Atcitty, "A comparison of diode-clamped and cascaded multilevel converters for a STATCOM with energy storage," *IEEE Trans. Ind. Electron.*, vol. 53, no. 5, pp. 1512–1521, Oct. 2006.

[8] A. K. Gupta and A. M. Khambadkone, "A space vector PWM scheme for multilevel inverters based on two-level space vector PWM," *IEEE Trans. Ind. Electron.*, vol. 53, no. 5, pp. 1631–1639, Oct. 2006.

[9] A. Chen and X. He, "Research on hybrid-clamped multilevel-inverter topologies," *IEEE Trans. Ind. Electron.*, vol. 53, no. 6, pp. 1898–1907, Dec. 2006.

[10] L. Yacoubi, K. Al-Haddad, L.-A. Dessaint, and F. Fnaiech, "Linear and nonlinear control techniques for a three-phase three-level NPC boost rectifier," *IEEE Trans. Ind. Electron.*, vol. 53, no. 6, pp. 1908–1918, Dec. 2006.

[11] A. Yazdani and R. Iravani, "An accurate model for the DC-side voltage control of the neutral point diode clamped converter," *IEEE Trans. Power Del.*, vol. 21, no. 1, pp. 185–193, Jan. 2006.

[12] A. R. Beig, G. Narayanan, and V. T. Ranganathan, "Modified SVPWM algorithm for three level VSI with synchronized and symmetrical waveforms," *IEEE Trans. Ind. Electron.*, vol. 54, no. 1, pp. 486–494, Feb. 2007.

[13] K. Jin, X. Ruan, and F. Liu, "An improved ZVS PWM three-level converter," *IEEE Trans. Ind. Electron.*, vol. 54, no. 1, pp. 319–329, Feb. 2007.

[14] P. Lezana, C. A. Silva, J. Rodriguez, and M. A. Perez, "Zero-steady-state-error input-current controller for regenerative multilevel converters based on single-phase cells," *IEEE Trans. Ind. Electron.*, vol. 54, no. 2, pp. 733–740, Apr. 2007.

[15] F. Liu and X. Ruan, "ZVS combined three-level converter—A topology suitable for high input voltage with wide range applications," *IEEE Trans. Ind. Electron.*, vol. 54, no. 2, pp. 1061–1072, Apr. 2007.

[16] C. Rech and J. R. Pinheiro, "Hybrid multilevel converters: Unified analysis and design considerations," *IEEE Trans. Ind. Electron.*, vol. 54, no. 2, pp. 1092–1104, Apr. 2007.

[17] A. Cataliotti, F. Genduso, A. Raciti, and G. Ricco Galluzzo, "Generalized PWM–VSI control algorithm based on a universal duty-cycle expression: Theoretical analysis, simulation results, and experimental validations," *IEEE Trans. Ind. Electron.*, vol. 54, no. 3, pp. 1569–1580, Jun. 2007.

[18] K. Jin and X. Ruan, "Zero-voltage-switching multiresonant three-level converters," *IEEE Trans. Ind. Electron.*, vol. 54, no. 3, pp. 1705–1715, Jun. 2007.

[19] J. Pou, J. Zaragoza, P. Rodriguez, S. Ceballos, V. M. Sala, R. P. Burgos, and D. Boroyevich, "Fast-processing modulation strategy for the neutral-point-clamped converter with total elimination of low-frequency voltage oscillations in the neutral point," *IEEE Trans. Ind. Electron.*, vol. 54, no. 4, pp. 2276–2287, Aug. 2007.

[20] Y. Suh, J. K. Steinke, and P. K. Steimer, "Efficiency comparison of voltage-source and current-source drive systems for medium-voltage applications," *IEEE Trans. Ind. Electron.*, vol. 54, no. 5, pp. 2521–2531, Aug. 2007.
[21] P. N. Tekwani, R. S. Kanchan, and K. Gopakumar, "A dual five-level inverter-fed induction motor drive with common-mode voltage elimination and DC-link capacitor voltage balancing using only the switching-state redundancy—Part I," *IEEE Trans. Ind. Electron.*, vol. 54, no. 4, pp. 2600–2608, Aug. 2007.
[22] P. N. Tekwani, R. S. Kanchan, and K. Gopakumar, "A dual five-level inverter-fed induction motor drive with common-mode voltage elimination and DC-link capacitor voltage balancing using only the switching-state redundancy—Part II," *IEEE Trans. Ind. Electron.*, vol. 54, no. 4, pp. 2609–2617, Aug. 2007.
[23] R. Vargas, P. Cortes, U. Ammann, J. Rodriguez, and J. Pontt, "Predictive control of a three-phase neutral-point-clamped inverter," *IEEE Trans. Ind. Electron.*, vol. 54, no. 5, pp. 2697–2705, Aug. 2007.
[24] S. Lakshminarayanan, G. Mondal, P. N. Tekwani, K. K. Mohapatra, and K. Gopakumar, "Twelve-sided polygonal voltage space vector based multilevel inverter for an induction motor drive with common-mode voltage elimination," *IEEE Trans. Ind. Electron.*, vol. 54, no. 5, pp. 2761–2768, Aug. 2007.
[25] S. Kouro, J. Rebolledo, and J. Rodriguez, "Reduced switching-frequency-modulation algorithm for high-power multilevel inverters," *IEEE Trans. Ind. Electron.*, vol. 54, no. 5, pp. 2894–2901, Aug. 2007.
[26] J. Holtz and N. Oikonomou, "Neutral point potential balancing algorithm at low modulation index for three-level inverter medium-voltage drives," *IEEE Trans. Ind. Appl.*, vol. 43, no. 3, pp. 761–768, Mar./Apr. 2007.
[27] B. A. Welchko, M. B. de Rossiter Correa, and T. A. Lipo, "A three-level MOSFET inverter for low-power drives," *IEEE Trans. Ind. Electron.*, vol. 51, no. 3, pp. 669–674, Jun. 2004.
[28] R. Teichmann and S. Bernet, "A comparison of three-level converters versus two-level converters for low-voltage drives, traction, and utility applications," *IEEE Trans. Ind. Appl.*, vol. 41, no. 3, pp. 855–865, May/Jun. 2005.
[29] A. Nabae, I. Takahashi, and H. Akagi, "A new neutral-point clamped PWM inverter," *IEEE Trans. Ind. Appl.*, vol. IA-17, no. 5, pp. 518–523, Sep./Oct. 1981.
[30] S. Ogasawara and H. Akagi, "Analysis of variation of neutral point potential in neutral-point-clamped voltage source PWM inverters," in *Proc. IEEE Ind. Appl. Soc. Annu. Meeting*, 1993, pp. 965–970.
[31] R. Rojas, T. Ohnishi, and T. Suzuki, "PWM control method for NPC inverters with very small dc-link capacitors," in *Proc. IPEC*, Yokohama, Japan, 1995, pp. 494–499.
[32] M. Cosan, H. Mao, D. Borojevic, and F. C. Lee, "Space vector modulation of three-level voltage source inverter," in *Proc. VPEC Semin.*, 1996, pp. 123–128.
[33] C. Newton and M. Sumner, "Neutral point control for multi-level inverters: Theory, design and operational limitations," in *Proc. IEEE Ind. Appl. Soc. Annu. Meeting*, 1997, pp. 1336–1343.
[34] D. H. Lee, S. R. Lee, and F. C. Lee, "An analysis of midpoint balance for the neutral-point-clamped three-level VSI," in *Proc. IEEE Power Electron. Spec. Conf.*, 1998, vol. 1, pp. 193–199.
[35] N. Celanovic and D. Boroyevich, "A comprehensive study of neutral-point voltage balancing problem in three level neutral-point-clamped voltage source PWM inverters," *IEEE Trans. Power Electron.*, vol. 15, no. 2, pp. 242–249, Mar. 2000.
[36] Z. Tan, Y. Li, and M. Li, "A direct torque control of induction motor based on three-level NPC inverter," in *Proc. IEEE Power Electron. Spec. Conf.*, 2001, vol. 3, pp. 1435–1439.
[37] J. Pou, D. Boroyevich, and R. Pindado, "New feedforward space-vector PWM method to obtain balanced ac output voltages in a three-level neutral-point-clamped converter," *IEEE Trans. Power Electron.*, vol. 49, no. 5, pp. 1026–1034, Oct. 2002.
[38] Q. Song, W. Liu, Q. Yu, X. Xie, and Z. Wang, "A neutral-point potential balancing algorithm for three-level NPC inverters using analytically injected zero-sequence voltage," in *Proc. IEEE Appl. Power Electron. Conf.*, 2003, vol. 1, pp. 228–233.
[39] S. Busquets-Monge, J. Bordonau, D. Boroyevich, and S. Somavilla, "The nearest three virtual space vector PWM—A modulation for the comprehensive neutral-point balancing in the three-level NPC inverter," *IEEE Power Electron. Lett.*, vol. 2, no. 1, pp. 11–15, Mar. 2004.
[40] S. Busquets-Monge, S. Somavilla, J. Bordonau, and D. Boroyevich, "Capacitor voltage balance for the neutral-point-clamped converter using the virtual space vector concept with optimized spectral performance," *IEEE Trans. Power Electron.*, vol. 22, no. 4, pp. 1128–1135, Jul. 2007.
[41] A. Mirecki, X. Roboam, and F. Richardeau, "Architecture complexity and energy efficiency of small wind turbines," *IEEE Trans. Ind. Electron.*, vol. 54, no. 1, pp. 660–670, Feb. 2007.
[42] H. du Toit Mouton, "Natural balancing of three-level neutral-point-clamped PWM inverters," *IEEE Trans. Ind. Electron.*, vol. 49, no. 5, pp. 1017–1025, Oct. 2002.
[43] J. J. Rodriguez-Andina, M. J. Moure, and M. D. Valdes, "Features, design tools, and application domains of FPGAs," *IEEE Trans. Ind. Electron.*, vol. 54, no. 4, pp. 1810–1823, Aug. 2007.

Sergio Busquets-Monge (S'99–M'01) was born in Barcelona, Spain. He received the degree in electrical engineering from the Technical University of Catalonia, Barcelona, Spain, in 1999, the M.S. degree in electrical engineering from Virginia Polytechnic Institute and State University, Blacksburg, in 2001, and the Ph.D. degree in electrical engineering from the Technical University of Catalonia, in 2006.

From 2001 to 2002, he was with Crown Audio, Inc. He is currently an Associate Professor with the Department of Electronic Engineering, Technical University of Catalonia, Barcelona, Spain. His research interests include multilevel conversion, power-converter modeling, control, and automated design, power-factor correction, and electromagnetic interference suppression techniques.

José Daniel Ortega was born in Ciutadella de Menorca, Spain. He received the degree in electrical engineering from the Technical University of Catalonia, Barcelona, Spain, in 2006.

Currently, he is with Adisa Calefacción, S. L., Barcelona.

Josep Bordonau (S'87–M'89) received the M.Sc. and Ph.D. degrees in electrical engineering (with honors) from the Technical University of Catalonia, Barcelona, Spain, in 1984 and 1990, respectively.

He is currently an Associate Professor with the Department of Electronic Engineering, Technical University of Catalonia. He has been active in more than 25 research projects with international companies and institutions. He is the author of many published articles. His fields of interest are multilevel conversion and ac power conversion applied to renewable-energy systems and energy-management systems.

José Antonio Beristáin was born in Veracruz, Mexico, in 1973. He received the B.Sc. degree in electronic engineering from the Technological Institute of Orizaba, Orizaba, Mexico, in 1995 and the M.S. degree from the National Center of Research and Technological Development, Cuernavaca, Mexico, in 1999, and the Ph.D. degree from the Technical University of Catalonia, Barcelona, Spain, in 2005.

He is currently an Associate Professor with the Technological Institute of Sonora, Sonora, Mexico, where he teaches and conducts research in power electronics. His research interests include high-frequency link multilevel inverters and power converters for nonconventional energy sources.

Joan Rocabert was born in Barcelona, Spain. He received the degree in electrical engineering from the Technical University of Catalonia, Barcelona, Spain, in 2003. He is currently working toward the Ph.D. degree in electrical engineering Technical University of Catalonia.

Since 2004, he has been a Researcher with the Department of Electronic Engineering, Technical University of Catalonia. His field of interest is power electronics applied to photovoltaic- and wind-energy systems.